TO BE SUBMITTED
TO NUOVO CIMENTO

CERN/TC/PHYSICS 66-6
26.4.1966.

Observation of spin alignment of resonances produced in the 3-body reactions : $\bar{p}p \to \bar{p}p\,\omega^0$ and $\bar{p}p \to \bar{N}^{*+++}\pi^0$ at 5.7 GeV/c

V. Alles-Borelli*), B. French, A. Frisk, L. Michejda**)

CERN - Geneva

Summary

The reaction $\bar{p}p \to \bar{p}p\,\pi^-\,\pi^+\,\pi^0$ has been studied at 5.7 GeV/c in the 81 cm Saclay hydrogen bubble chamber. Production of ω^0 and η^0 mesons has been observed. The ω^0 mesons are collimated in the forward and backward directions in the c.m.s. The decay angular distribution of the ω^0 indicates that it is produced with the spin aligned in the plane perpendicular to the incident $\bar{p}$ (or p) momentum transformed to the ω^0 rest frame, an effect which is enhanced when the four-momentum transfer t is limited to $|t| < 0.5\ (\mathrm{GeV/c})^2$.

It has been found that of the observed $N^{*+++}(1238)$ and $\bar{N}^{*---}(1238)$ isobars about 80 o/o are produced in pairs in the 3-body reaction $\bar{p}\,p \longrightarrow \bar{N}^{*---}\,N^{*+++}\,\pi^0$. In this reaction the N^* isobars are produced in aligned states with the spin directions of the N^* and $\bar{N}^*$ being strongly correlated such that there are few events in which both the N^* and $\bar{N}^*$ decay with the p and $\bar{p}$ from the isobars making large angles relative to initial p or $\bar{p}$ direction transformed into the isobar rest frame.

---

*) Now at the Institute of Physics, Bologna.

**) On leave of absence from Institute of Nuclear Research, Warsaw.

1. Experimental procedure and cross section

Four-prong events produced by a 5.7 GeV/c separated antiproton beam in the Saclay 81 cm hydrogen bubble chamber have been measured with the CERN HPD system. 19,100 events without visible strange particle production were accepted for further analysis. A detailed study of the HPD measurements has shown that their quality is not inferior to that of conventional IEP measurements[1][2]. Analysis of a sample of the 11 o/o of the attempted events, which did not pass successfully through the system, show no special features which could introduce a bias into the accepted sample of 19,100 events[2].

The standard CERN chain of programs was used to reconstruct and analyse the measured events. Ionisation measurements, which were automatically supplied by the HPD for all events, were used to help in choosing the right interpretation between different kinematical fits.

The events without neutral particles in the final state, 4 constraint (4C) fits, were separated out provided the kinematical probability P (χ^2_{4C}) was greater than 1 o/o and if ionisation was in agreement with the chosen hypothesis.

In the present paper we discuss the following 1 - constraint (1C) channel :

$$\bar{p}p \longrightarrow \bar{p}p \quad \pi^+ \pi^- \pi^o \qquad (1)$$

All events having kinematical fits to (1) with a probability P (χ^2_{1C}) greater than 1 o/o were considered as candidates for this reaction. A total probability, defined as the normalized product of the kinematical probability and an ionisation probability obtained from the ionisation fit described in reference[3], was computed for all these events. Fits having a total probability larger than 1 o/o were accepted by the programs and the decisions

checked by physicists at a scanning table.

1742 events were accepted which had a unique fit to the channel (1). 570 events for which a second fit was also possible were analysed separately. It was found that the production c.m. angular distributions for particles and antiparticles become consistent with C conservation requirements only after including these 570 events into the sample of unambiguous events. In addition the production rate of ω^o mesons in the ambiguous sample was found to be as high as in the unambiguous events. Therefore in the following analysis we consider the total sample of 2312 events as belonging to reaction (1). Another 127 events (5 o/o of the accepted events) which had 3 possible 1C fits were not considered but the cross section for channel (1) was arbitrarily corrected by an amount corresponding to half of them.

The cross section for 4-prong stars without visible strange particles has been determined by track and interaction counting in 4 o/o of the available film. After correcting for beam contamination (6 o/o of μ^- and 2 o/o of π^- mesons) we obtained :

$$\sigma \text{ (4 prong)} = (17.3 \pm 0.7) \text{ mb.}$$

Thus the cross section corresponding to 1 event in our sample is (0.910 ± 0.037) μb. Using this value and the data discussed above the cross section for the channel (1) has been determined to be

$$\sigma = (2.16 \pm 0.14) \text{ mb.}$$

The quoted error includes statistical errors, errors due to the uncertainties of the corrections applied and the uncertainty in the separation of channel (1) from the other possible channels. From the χ^2 distribution and the symmetries observed in the particle angular distributions we estimate that the sample of 2312 events does not contain more than 5 o/o of contaminating events.

2. Production of ω^o in the 3-body reaction $\bar{p}p \rightarrow \bar{p}p\,\omega^o$ and its decay.

2. 1) Cross sections for production of mesonic resonances.

The mass distribution for the neutral 3-pion system from the channel (1) is shown in Fig. 1. One sees clearly the ω^o and η^o peaks. The smooth curve normalized to all events except the ω^o and η^o combinations has been drawn by hand. The phase space distribution differs slightly in that it predicts fewer events at low masses and more at high masses than observed. The resolution function for the ω mesons has been constructed from individual mass errors for the 3π combinations from the peak region. It is well approximated by a Breit-Wigner curve with a width $\Gamma_{res} = 32$ MeV, compared to which the intrinsic width of the ω^o meson may be neglected. The region of the ω^o peak (685 MeV - 880 MeV) was then fitted with a least squares method to a straight line plus a Breit-Wigner curve and gave the following mass and width values

$$M_{\omega o} = (780.9 \pm 2.0) \text{ MeV} \quad ,$$

$$\Gamma_{\omega o} = (\ 29 \pm 5) \text{ MeV} \quad ,$$

and a cross section for ω^o production

$$\sigma_{\omega o} = (233 \pm 36)\ \mu b \ .$$

The error comes mainly from the uncertainty in separating the peak from the background.

The cross section for η^o production is estimated to be

$$\sigma_{\eta o} = (43 \pm 8)\ \mu b \ .$$

The cross sections $\sigma_{\omega o}$ and $\sigma_{\eta o}$ include only the observed $\pi^+ \pi^- \pi^o$ decay mode.

We conclude that the cross section for ω^o production has increased considerably compared to the value of 60 ± 20 μb reported at 3.6 GeV/c[4]. Weak evidence for η^o production in the 3-4 GeV/c region has been reported

by T. Ferbel et al.[5]. In pp interactions at about 3 GeV/c observations of ω^o[6] and η^o[7] production has been reported.

Further discussion of the channel

$$\bar{p}p \rightarrow \bar{p}p \ \omega^o \qquad (2)$$

will be restricted to the 253 events having a 3-pion mass lying in the region

$$760 \text{ MeV} < M(\pi^+ \pi^- \pi^o) < 805 \text{ MeV} .$$

The estimated number of $\pi^+ \pi^- \pi^o$ combinations in this region not arising from ω^o decay is 89 events (i.e. 35 o/o of all events). As a control region for a production angular distribution study we will use the following adjacent bands of the $\pi^+ \pi^- \pi^o$ mass spectrum : 715-760 MeV and 805-850 MeV, where we expect about 30 o/o of the events to be genuine omegas. The bands are narrow enough to avoid the influence of a dependence of the angular distribution on mass which we find for the background. For the study of decay distributions, where we do not find a dependence on mass, we enlarged these bands to 670-760 MeV and 805-895 MeV where the percentage or omegas is reduced to 19 o/o.

2. 2) Properties of ω^o meson production.

In this section we discuss general features of ω^o production in reaction (2).

The production angular distribution is shown in Fig. 2. The histogram for the peak region is drawn with a full line and compared with the angular distribution of the $\pi^+ \pi^- \pi^o$ combinations from the adjacent regions (dashed line). We conclude that there is a strong forward-backward collimation of ω^o mesons which is somewhat weaker for the background events.

A Dalitz plot for the 253 $\bar{p}p \ \omega^o$ final states is shown in Fig. 3. There is a tendency for the ω^o meson to make a small mass with one of the

nucleons. The broad enhancements of the $p\omega$ or $\bar{p}\omega$ mass in a region of about 1.80 GeV is more easily seen in the mass distribution shown in Fig. 4 (b), where it is compared with a phase space curve. The Chew-Low plot of Fig. 4 (a) demonstrates that these small masses correspond to small momentum transfers between the incident $\bar{p}$ or the target p and the $\bar{p}\omega^o$ or $p\omega^o$ system respectively, which is however a general tendency observed for higher masses as well.

We are not tempted to interpret the enhancement at 1.8 GeV in terms of a possible nucleon isobar since (a) there is no known isobar in the region of about 1.8 GeV and it is not very probable that the tail of the $N^*_{1/2}(1688)$ would be still important there and (b) 3π combinations of similar masses but not coming from ω^o decay show a similar feature.

A more plausible interpretation seems to be in terms of a peripheral production mechanism for the ω^o.

2. 3) Observation of ω^o spin alignment.

Tempted by peripheral features of the ω^o production in a search for a possible spin alignment of the ω^o meson we used as a quantization axis the incident antiproton or the target proton directions Lorentz transformed into the ω^o rest frame.

To decide which of them, $\bar{p}$ or p, has to be used we compared the final state $\bar{p}\omega$ and $p\omega$ masses and chose the particle corresponding to a smaller mass. Other possible selection criteria based on c.m. production angle of the omega or smaller t-value give similar results.

As an analyser we used the normal to the ω^o decay plane which on the average lies perpendicular to the ω^o spin direction.

Fig. 5 (a) shows the distribution $\cos\Theta'$ of the angle between the normal to the ω^o decay plane and the $\bar{p}$ or p direction in the ω^o rest system

for the 253 events in the ω^o mass interval. The distribution is anisotropic and indicates that the decay plane lies preferentially perpendicular to the $\bar{p}$ or p momentum direction. A fit to this distribution, using a least squares method, of the following equation

$$\frac{N}{2 + 2/3\ B} \quad (1 + B \cos^2\theta') \qquad (3)$$

where N in the normalization factor is a number of events in the histogram, yields a value of $B = 1.05 \pm 0.44$. The shaded area shows the distribution for events in the adjacent regions 670-760 MeV and 805-895 MeV normalized to 89 events which correspond to the estimated $\pi^+ \pi^- \pi^o$ background in the ω^o peak region. After subtraction of the background, which is consistent with isotropy, the net distribution may be described by (3) with a coefficient $B = 1.53 \pm 0.59$.

These data indicate that the ω^o mesons are produced with their spins strongly aligned in the plane perpendicular to the direction of the incident $\bar{p}$ or the target p, and having a spin projection along the p or $\bar{p}$ direction equal to zero in (56 ± 6) o/o of events. Isotropy would require the spin projection to be zero in 1/3 of the events only.

This effect of alignment is almost complete for events where the $p\omega$ or $\bar{p}\omega$ systems have small masses or where they have small momentum transfers relative to the target p or the incident $\bar{p}$. This can be seen in Figs. 5 (b) and 5 (c) where both selections have been applied. Even without subtracting flat background the fitted B parameters in (3) are then 1.71 ± 0.72 and 1.90 ± 0.81 respectively.

If we consider a one particle exchange mechanism, as e.g. the one shown in Fig. 6 (a), it is important to see what is the ω angular distribution in the rest frame of the $\bar{p}\omega$ or $p\omega$ system relative to the incident $\bar{p}$ or the target p momentum transformed to the $\bar{p}\omega$ or $p\omega$ system taken as z-axis, and the

normal to the $\bar{p}\omega$ or $p\omega$ production plane taken as y-axis. The distribution of the Treiman-Yang angle is flat, as required for zero-spin exchange, and the polar angular distribution, while being symmetric about $\cos\theta = 0$ as required for an isobar decay shows also a slight forward-backward peaking. A fit to the formula (3) for events with M ($\bar{p}\omega$) or M ($p\omega$) smaller than 1.88 GeV yielded $B = 0.95 \pm 0.53$, where subtraction of the background has not been attempted due to poor statistics.

Kraemer et al. studying the reaction

$$\pi^+ n \rightarrow \omega^o p$$

near threshold found a strong alignment of the ω^o spin [6]. They used a z-quantization axis along the incident π^+ meson momentum Lorentz transformed into the ω^o rest frame. Their distribution of the angle which the normal to the ω^o decay plane makes with this axis is consistent with a cosine-squared form ($B = 2.1 \pm 0.7$). A similar observation ($B = 1.8 \pm 0.5$) has been reported also at 1.7 GeV/c π^+ momentum, (2.0 GeV c.m. energy), by Bacon et al.[9].

One could try to compare these data with the present observation assuming that, in the one particle exchange graph shown in Fig. 6 (a) the exchanged particle is really a π^o. Then the process in the upper vertex of the graph is

$$\pi^o \bar{p} \rightarrow \omega^o \bar{p}$$

similar to that observed by Kraemer et al. and therefore a corresponding angle could be easily defined. If in addition the $\bar{p}\omega^o$ system forms an isobar a natural choice for the ω^o spin quantization axis would be the momentum of the incident $\bar{p}$ transformed into the $\bar{p}\omega$ rest frame since an isobar with spin $J > 1/2$ produced according to Fig. 6 (a) would be aligned with respect to this axis and could transmit its alignment to the ω^o.

Therefore we studied the ω^o alignment along these two new quantization axes : 1) the direction of the virtual π^o momentum transformed into the ω^o rest frame, and 2) the incident $\bar{p}$ momentum direction transformed into the $\bar{p}\omega^o$ rest frame. The result is that none of them gives as strong an effect as that observed for the axis which we used previously. On the other hand the new cos θ' distributions have shapes similar to that showed in Fig. 5 (a) and the statistics available does not allow us to distinguish which is the real effect and what is only its reflection. Nor are we able to explain the mechanisms producing ω^o alignment in the present experiment and those of Kraemer et al. and Bacon et al., which could possibly be the same.

An interpretation of the $\pi^+ n$ data in terms of a ρ - exchange model with absorption corrections has been suggested by Bacon et al. . A simple ρ - exchange model (in the reaction $\bar{p}p \rightarrow \bar{p}p\omega^o$ would mean a double peripheral model with both π^o and ρ^o exchange as shown in Fig. 6 (b)) predicts for the ω^o, as discussed by Kraemer et al., a $\sin^2\theta'$ decay distribution in disagreement with the data. Only after "correcting" for absorption effects does it become equal to $1 + 2\cos^2\theta'$ as observed experimentally, a quite surprising result as the "corrections" turned out to be more important than the basic Born term prediction.

3. The 3-body reaction $\bar{p}p \to \bar{N}^{*--} N^{*++} \pi^o$

3. 1) Cross section for an associated production of the $N^*(1238)$, $\bar{N}^*(1238)$ isobars.

We now pass to the evidence indicating the existence of the following channel :

$$\bar{p}p \to \bar{N}^{*--} N^{*++} \pi^o \qquad (4)$$

In the Fig. 7 the mass of the $p\pi^+$ system versus the mass of the $\bar{p}\pi^-$ system is plotted for the 2009 events outside the ω^o and the η^o regions. (The η^o-region was chosen as the 45 MeV interval from 525 MeV to 570 MeV). There exists an important clustering of points in the region where the $N^*(1238)$ and $\bar{N}^*(1238)$ bands overlap.

The amount of associated and single $N^*(1238)$ production has been determined by applying a maximum likelihood fitting procedure to the 2-dimensional distribution of Fig. 7. The 5-body problem has been reduced to a 4-body one by considering only $\bar{p}p\,\pi^+\,\pi^-$ substates with experimentally observed invariant masses W_i. Compared with the analoguous fitting of the channel without $\pi^{o(10)}$ there is one complication : each event has a different π^o energy and therefore the total energy W_i left to 4-particle system $\bar{p}p\,\pi^+\,\pi^-$ studied in Fig. 7 is not constant.

In the likelihood function the probability distribution for the i^{th} event had a form analoguous to that used by Ferro-Luzzi et al.[11] :

$$\varphi^i(M_{p\pi^+}, M_{\bar{p}\pi^-}) = f_{N^*\bar{N}^*} F^i_{N^*\bar{N}^*} + f_{N^*} F^i_{N^*} + f_{\bar{N}^*} F^i_{\bar{N}^*} + (1 - f_{N^*\bar{N}^*} - 2 f_{N^*}) \times F^i_{\bar{p}p\,\pi^-\pi^+}, \qquad (5)$$

where the four terms correspond to the following final states :

$$N^* \bar{N}^* \pi^o \quad \text{(3 bodies)} \qquad (6)$$

$$N^* \bar{p}\,\pi^-\,\pi^o \quad \text{(4 bodies)} \qquad (6a)$$

$$p\pi^+ \bar{N}^*\,\pi^o \quad \text{(4 bodies)} \qquad (6b)$$

$$p\pi^+ \bar{p}\pi^- \pi^o \qquad (5 \text{ bodies}) \qquad (6c)$$

The parameters $f_{N^*\bar{N}^*}$ and $2f_{N^*}$ in (5) are the frequencies of double and single isobar production which we would like to determine. In the four distributions F^i we have assumed a relativistic Breit-Wigner distribution for the N^* isobars which has a p-wave energy dependence of the width according to the formula A2 in the Appendix of the paper by Ferro-Luzzi et al.[11]. The appropriate 2 -, 3 - and 4 - body phase space factors were also used.

The likelihood function was a product of the 2009 (number of events) probability distributions $\varphi^i (M_{p\pi^+}, M_{\bar{p}\pi^-})$ normalized over the allowed kinematic triangles and where the experimental values $(M^i_{p\pi^+}, M^i_{\bar{p}\pi^-})$ were substituted into the corresponding terms. The width was fixed and equal to $\Gamma = 120$ MeV while the N^* mass M was allowed to vary to account for its possible shift from the accepted value.

The fitting procedure determined the frequencies of double and single isobar production :

$$\begin{aligned} f_{N^*\bar{N}^*} &= 0.292 \pm 0.022 \quad , \\ f_{N^*} &= 0.073 \pm 0.020 \quad , \qquad (7) \\ (M_{N^*} &= 1222 \pm 2 \text{ MeV}) \quad . \end{aligned}$$

The two projections of the fitted 2-dimensional mass distribution on to the $M(p\pi^+)$ and $M(\bar{p}\pi^-)$ mass axes are shown in Fig. 8 where they are compared with the experimental histograms. It is clear that the fit is quite good and a χ^2 test applied to the combined mass distribution gives a probability of 10 o/o.

The fit discussed above was based on the following assumptions :

1) The 4 channels (6), (6a), (6b) and (6c) do not interfere with each other (but even allowing for a maximum constructive interference of the N^*, $\bar{N}^*$ bands in the overlap region the fraction $f_{N^*\bar{N}^*}$ in (7) drops only to about 25 o/o).

2) C is conserved (as the parameters characterising N^{*} and $\bar{N}^{*}$ were assumed to be equal).

3) The phase space mass distributions are adequate to describe mass distributions for 4 and 5 body channels (6a), (6b) and (6c).

We feel that the weakest assumption is the last. The uncertainty in the shape of mass distribution is not taken into account in the errors calculated for the fit as given in (7). We think it is reasonable to multiply the errors on frequencies (7) by a factor of 2 in order to account for possible deviations of the mass spectra from the phase space mass distributions used in (5).

After making corrections for the events containing uncorrelated $\pi^{+}\pi^{-}\pi^{o}$ triplets in the ω^{o} and η^{o} regions the fitted frequencies (7) were used to determine the cross section for single and double $N^{*}(1238)$ production in the channel (1). They are equal to :

$$\sigma\ (\bar{p}p \rightarrow \bar{N}^{*--}\ N^{*++}\ \pi^{o}) = 580 \pm 95\ \mu b\ ,$$

$$\sigma\ (\bar{p}p \rightarrow \bar{N}^{*--}\ p\pi^{+}\ \pi^{o}) = \sigma\ (\bar{p}p \rightarrow \bar{p}\pi^{-} N^{*++}\ \pi^{o}) = 145 \pm 80\ \mu b\ .$$

As can be seen in Fig. 9 (b) the c.m.s. angular distribution of the π^{o} mesons is reasonably symmetric with respect to $\cos\theta = 0$ which is an indication that no important biases are present.

It seems striking that about 80 o/o of $N^{*}(1238)$ isobars observed in the channel (1) are produced in the 3-body final state (6). This preference of the isobars to be produced in pairs may explain why in the range of 3-4 GeV/c antiproton momenta, which are close to threshold for the associated production, little or no N^{*} isobar production was observed in this channel[4][5].

In the following study of the reaction (6) we will confine the discussion to those events which have both the $M(p\pi^{+})$ and $M(\bar{p}\pi^{-})$ masses lying inside the interval 1.16 - 1.28 GeV. In choosing such a restricted mass

interval we will have the advantage of dealing with a relatively clean sample. Namely, out of 313 events coming from the described region we expect 229 to represent genuine $N^{*}\bar{N}^{*}\pi^{o}$ events, 31 single N^{*} production events and 53 five-body events. We will subtract the "background" by using the 567 events which have both masses $M(p\pi^{+})$ and $M(\bar{p}\pi^{-})$ smaller than 1.4 GeV but not lying inside the square 1.16 - 1.28 GeV x 1.16 - 1.28 GeV. In this sample $\bar{N}^{*}$ N^{*} π^{o} production represents about 37 o/o of the events.

3. 2) General properties of the N^{*} $\bar{N}^{*}$ π^{o} final state.

We will now discuss the properties of reaction (6) using the 313 events which, in Fig. 7 are located in the square in which both the $M_{p\pi^{+}}$ + $M_{p\pi^{-}}$ - masses lie in the interval 1.16 GeV to 1.28 GeV.

Fig. 9 shows the c.m. angular distributions for N^{*}'s , π^{o} mesons and $\bar{N}^{*}$'s . One notices a strong peaking of the isobars and a small anisotropy in the π^{o} distribution. The presence of a small bias indicated by the asymmetry of the π^{o} angular distribution and the difference in the N^{*} and reflected $\bar{N}^{*}$ distributions, is expected to have little influence in the following discussion.

In Fig. 10 a Dalitz plot for the $\bar{N}^{*}N^{*}$ π^{o} final state is shown and in Fig. 11 a projected mass distribution of the $\bar{N}^{*--}$ π^{o} and $N^{*++}\pi^{o}$ systems is compared with the phase space curve. There is an excess of events in the lower mass region which seems difficult to explain in terms of one or two well established nucleon isobars. On the other hand the angular distributions shows that this reaction has a strongly peripheral character and as a consequence one could then expect a broad enhancement in the small mass region.

As a conclusion from the above discussion in the next Section we will assume a peripheral graph with 2 or 3 vertices : the upper vertex producing the $\bar{N}^{*}$ and the lower vertex the N^{*} .

3. 3) Spin alignment and decay correlation of the N^{*} and $\bar{N}^{*}$ isobars.

We define the angle θ' as the angle between the momentum of the $\bar{p}$ from the $\bar{N}^{*}$ decay and the incident antiproton momentum transformed into the $\bar{N}^{*}$ rest frame considered as z-axis. The normal to the production plane of N^{*} is taken as y-axis which fixes the azimuthal angle ϕ_{TY}. Corresponding angles are also defined for the N^{*} isobars. In the various angular distributions presented the background has been always subtracted since it was found to behave differently from the genuine $N^{*}\bar{N}^{*}\pi^{o}$ events. The background distributions were obtained by using the 567 events from adjacent regions as described in Section 3.1. These distributions were always normalized to the estimated number of 101 background events which, when subtracted from the sample of 313 events, are assumed to leave 212 clean $N^{*}\bar{N}^{*}\pi^{o}$ events. The distributions of the background will be indicated to show what difference this subtraction procedure makes.

The angular distribution of θ' for all N^{*} and $\bar{N}^{*}$ isobars is shown in Fig. 12 (a) as a full line and a slight anisotropy is apparent which may be expressed by the value of the coefficient B of formula (3). This coefficient was found, with a least squares method, to be $B = 0.47 \pm 0.27$. The background events are peaked forwards as is shown (dashed line histogram of Fig. 12 (a)).

The observed anisotropy might be explained by using the graph shown in Fig. 13 (a). Assuming pion exchange one could expect that one of the N^{*}'s will be produced in an aligned state as for example is observed for both isobars in the 2-body reaction $\bar{p}p \rightarrow N^{*}\bar{N}^{*}$ (7). This results from the fact that the isobars are produced with their spin projections along the direction of corresponding incident nucleon equal to $\pm 1/2$. The decay distributions is then predicted to be of the form : $1 + 3\cos^{2}\theta'$. On the other hand the

absorption corrections (see Svensson's calculations[12]) destroy this high alignment reducing the anisotropy to $1 + 0.7 \cos^2 \theta'$ observed experimentally[10]. The observed value of $B = 0.47 \pm 0.27$ is consistent with the hypothesis of 0-spin exchange if we assume that the N^{*} produced at the π^{o} vertex (Fig. 13(a)) would produce an isotropic decay angular distribution and that the absorption corrections are as strong as in the 2-body process $\bar{p}p \rightarrow N^{*} \bar{N}^{*}$. To check further the possibility that the graph shown in Fig. 13 (a) plays an important role in the studied channel (6) we have tried to separate the events where the π^{o} meson is produced in the upper vertex and the N^{*} is emitted "free" from the events where the π^{o} is produced in the lower vertex and the $\bar{N}^{*}$ is produced "free". In this attempt we have neglected a possible interference between the conjugated graphs and used as in the ω case the criterion of a smaller mass applied now to the masses of the $\bar{N}^{*} \pi^{o}$ and the $N^{*} \pi^{o}$ systems. Namely, for the events where $M(N^{*} \pi^{o}) < M(\bar{N}^{*} \pi^{o})$ we assume that the π^{o} is produced in the lower vertex and the $\bar{N}^{*}$ is "free" and for the events where $M(N^{*} \pi^{o}) > M(\bar{N}^{*} \pi^{o})$ we assume that the π^{o} is produced in the upper vertex and the N^{*} is produced "free".

The results of this separation procedure are presented in Fig. 12 (b) where the lower and upper histograms show the decay angular distributions for "free" isobars and the isobars which are considered as being produced in the π^{o} vertex respectively. There seems to be a dependence in the predicted sense. The values of the B coefficients are respectively 0.95 ± 0.51 and 0.21 ± 0.31, but the significance of the observed differences of these values from the expected value (0.47 ± 0.38) corresponds to 1.4 standard deviations only. The "free" isobar distribution of the azimuthal Treiman-Yang angle defined at the beginning of this Section is uniform in accordance with a 0-spin exchange model.

However we now present an effect which is not readily explained by the graph of Fig. 13 (a). Following Ref. (13) we looked for a possible correlation between the decays of the N^{*} and the $\bar{N}^{*}$ isobars. Thus the lower and upper histograms of Fig. 12 (c) show the distribution of cos θ'_1 for those isobars in which the absolute value of cos θ'_2 of the other isobar is less or greater than 0.5, respectively.

If there were no correlation between the decays of the N^{*} and $\bar{N}^{*}$ isobars both distributions should be equal within errors to the overall distribution presented in Fig. 12 (a), with B = 0.47 ± 0.41 and 0.47 ± 0.36, where the errors are predicted from the known number of events in both distributions and include errors due to background subtraction. The experimental distributions of Fig. 12 (c) are different from each other, the fitted values of the parameter B being 1.74 ± 0.83 and 0.00 ± 0.23 for the lower and upper histograms of Fig. 12 (c) respectively. A one degree of freedom χ^2 test for the "no correlation" hypothesis gives $\chi^2 = 11.3$ and corresponds to 3.4 standard deviations. We may consider it proven that a correlation exists between the decay of the N^{*} and the decay of the $\bar{N}^{*}$ isobars in the channel (6). It is important to notice that a weak correlation which seems to exist in the quasi-two-body reaction $\bar{p}p \rightarrow \bar{N}^{*--} N^{*++}$ (10) has the opposite trend and could be explained as due to absorption corrections of the π-exchange mechanism[12].

It should be noted that the graph of Fig. 13 (a) when mixed with its charge conjugate graph and with the assumptions previously discussed predicts a small correlation between the 2 decays. The joint, 2-dimensional decay distribution may be written as

$$\underline{\phi}\,(\cos\theta'_{N^{*}}, \cos\theta'_{\bar{N}^{*}})\, d\cos\theta'_{N^{*}}\, d\cos\theta'_{\bar{N}^{*}} =$$
$$= \left[(1 + 1.11\cos^2\theta'_{N^{*}}) + (1 + 1.11\cos^2\theta'_{\bar{N}^{*}})\right] d\cos\theta'_{N^{*}}\, d\cos\theta'_{\bar{N}^{*}}\,, \quad (8)$$

where the first torm in the right-hand side square parenthesis corresponds to the "free" aligned N^{*} and isotropically decaying $\bar{N}^{*}$ and the second term corresponds to the aligned $\bar{N}^{*}$ and anisotropically decaying N^{*}. The coefficient 1.11 has been computed such that after integration of (8) over one of the angles one obtains the overall observed angular distribution $1 + 0.47 \cos^2 \theta'$. The B coefficients and their predicted errors corresponding to the two experimental distributions shown in Fig. 12 (c) can be calculated from the formula (8) and they are $B = 0.53 \pm 0.41$ (for $|\cos\theta_2| < 0.5$) and $B = 0.42 \pm 0.36$ (for $|\cos\theta_2| > 0.5$). It is clear that the observed correlation is much stronger and significantly (3 standard deviations) different from the predicted amount.

We could expect that the small correlation predicted by (8) would be eliminated if we studied not a joint angular distribution where the $\cos \theta'$ of N^{*} is considered versus the $\cos \theta'$ of $\bar{N}^{*}$ but instead the $\cos \theta'_1$ of the isobar which makes a larger mass with the π^{o} ("free" isobar in the graph of Fig. 13 (a)) versus the $\cos \theta'_2$ of the isobar which makes a smaller mass with the π^{o} (isobar produced in the π^{o} vertex in Fig. 13 (a)). In Fig. 14 we show such a scatter diagram together with projections made separately for 2 intervals of $\cos \theta'$ of the partner isobars. All 313 events are plotted in the scatter plot but in the projections background distributions have been subtracted and are marked with a dashed line. Least squares fits for the parameter B of formula (3) gave the following values

$$B\ (\cos \theta'_1) = 2.13 \pm 1.26 \text{ for } |\cos \theta'_2| < 0.5$$

$$B\ (\cos \theta'_1) = 0.38 \pm 0.45 \text{ for } |\cos \theta'_2| > 0.5$$

$$B\ (\cos \theta'_2) = 1.32 \pm 0.94 \text{ for } |\cos \theta'_1| < 0.5$$

$$B\ (\cos \theta'_2) = -0.26 \pm 0.25 \text{ for } |\cos \theta'_1| > 0.5$$

It is clear that the correlation which can be noticed as the lack of events in the middle of the scatter diagram is not dependent on the specific separation of isobars.

The observed correlation shows that decay of both isobars under large angles is very improbable, but when one of them decays under a small angle the decays of its partner under large angles are not suppressed. In the reference frame previously described this means that states in which both isobars have projections on the z-axes (determined by incident particles) equal to $\pm$ 3/2 tend to be suppressed.

The only explanation of these data which we could think of requires the introduction of the double peripheral graph shown in Fig. 13 (b). Supposing that the Stodolsky-Sakurai model[14] is valid for the $N\rho N^{*}$ vertex and neglecting any absorption corrections, we can write down the joint decay probability distribution corresponding to the graph from Fig. 13 (b) and its charge conjugate as follows

$$\overline{+}\,(\cos\theta'_{N^{*}}, \cos\theta'_{\bar{N}^{*}})\, d\cos\theta'_{N^{*}}\, d\cos\theta'_{\bar{N}^{*}} =$$

$$= \left[(5 - 3\cos^2\theta'_{N^{*}})(1 + 3\cos^2\theta'_{\bar{N}^{*}}) + (5 - 3\cos^2\theta'_{\bar{N}^{*}})(1 + 3\cos^2\theta'_{N^{*}})\right] d\cos\theta'_{N^{*}}\, d\cos\theta'_{\bar{N}^{*}}$$

Terms of the form $5 - 3\cos^2\theta'$ describe the decay angular distribution of isobars produced in the $N\rho N^{*}$ vertices, while the terms $1 + 3\cos\theta'$ correspond to isobars produced in the $N\pi N^{*}$ vertices. The former have a bump for large angles and the latter give a forward-backward peaking with a dip at $\cos\theta' = 0$. Approximately speaking for each event one isobar is predicted to decay under a small angle and one under a large angle. As we see this correlation is qualitatively observed experimentally. In terms of the graphs of Fig. 13 (b) the result of stronger anisotropy for isobars making small masses with the π^{o} meson

could be understood if we assume that smaller (larger) momentum transfers correspond to the pion (ρ) internal line. This could be then followed by a tendency for the ρ-vertex isobars to make smaller masses with π^o mesons.

A prediction of the graph shown in Fig. 13 (b), assuming the Stodolsky-Sakurai model for the $N\rho N^{*}$ vertex, is that the azimuthal decay distribution of the isobars should be of the form

$$\varphi\left(\underline{\phi}\right) d\underline{\phi} = \left(1 + 2/3 \sin^2 \underline{\phi}\right) d\underline{\phi}$$

where the $(1 + 2 \sin^2 \underline{\phi})$ distribution for the N^{*} coming from the ρ-vertex has been combined with a uniform distribution for N^{*} coming from the π-vertex.

We have computed a new azimuthal angle which is appropriate to the upper part of the graph given in Fig. 13 (b) by making a transformation of all momenta into the c.m. system of the virtual collision $\pi^- \bar{p} \rightarrow \bar{N}^{*--} \pi^o$ and defining the normal to the production plane for this process. This direction was used in the $\bar{N}^{*--}$ rest frame as the y-axis, while the transformed $\bar{p}$ momentum direction served as the z-axis.

The experimental distribution of this angle is flat and when fitted with a least squares method to the form

$$\frac{N}{(C + 2)\,\pi} \left(1 + C \sin^2 \underline{\phi}\right)$$

yields a C value of 0.1 ± 0.2 in contradiction with the expected value of 0.66.

Therefore the model seems to us unlikely to explain the data. However one has to know how much the absorption corrections modify the alignment produced by the double peripheral model before making any final conclusions.

4. Conclusions

The two 3-body final states : $\bar{p}p \rightarrow \bar{p}p\omega^o$ and $\bar{p}p \rightarrow N^{*}\bar{N}^{*}\pi^o$ make important contribution to the 5-body reaction $\bar{p}p \rightarrow \bar{p}p\,\pi^+\,\pi^-\,\pi^o$, accounting for 11 o/o and 30 o/o respectively of the cross section of 2.16 ± 0.14 mb for this reaction. Compared to the data at lower energies[4][5] the ω^o production cross section has increased by a factor of four.

Both 3-body processes apparently reveal strongly peripheral characteristics and any suggested production mechanism must explain the observed strong spin alignment of the ω^o meson and the N^{*}, $\bar{N}^{*}$ isobars.

In the $\bar{p}p \rightarrow \bar{p}p\omega^o$ process the omegas are produced preferentially (56 o/o) with a spin projection of zero along the incident particle momentum direction. The spin alignment is almost complete for those events having small $p\omega^o$ or $\bar{p}\omega^o$ masses or produced with small momentum transfers. Both the alignment presently observed and the ω^o alignment reported in the reaction $\pi^+ n \rightarrow p\omega^o$ could possibly be due to the same production mechanism.

A strong correlation between the decays of the N^{*} and the $\bar{N}^{*}$ isobars was found in the channel $\bar{p}p \rightarrow N^{*}\bar{N}^{*}\pi^o$. The correlation is such that when one of the isobars decays with a large angle the other isobar tends to decay at a small angle relative to the incident nucleon momentum direction. A possible explanation in terms of a double peripheral model involving π and ρ exchange has been attempted but a disagreement in a Treiman-Yang angle distribution and the lack of information about the influence of absorption on the spin alignment does not allow to reach firm conclusions about the validity of the model.

5. Acknowledgments.

We acknowledge the assistance of the CERN proton synchrotron staff, members of the CERN TC Division who built the separated beam and the 81 cm Saclay bubble chamber crew. We would like to thank A. Accensi, J.M. Howie, W. Krischer, W.G. Moorhead, B.W. Powell, P. Seyboth and P. Villemoes without whose efforts the automatic measurements would not have been possible. We thank also the HPD personnel and our scanners for their efficient and careful work. We are grateful for the support given to us by Dr. R. Armenteros and Prof. Ch. Peyrou. One of the authors (L.M.) wishes to thank Prof. Ch. Peyrou for the hospitality extended to him at the CERN TC Division.

REFERENCES

1) A. Accensi, V. Alles-Borelli, B. French, Å. Frisk, J.M. Howie, L. Michejda, W.G. Moorhead, B.W. Powell, P. Villemoes, Proceedings of the Conference on Programming for Flying Spot Devices at Columbia University, October 1965.

2) P. Villemoes, CERN Yellow Report 66-4.

3) L. Michejda, Proceedings of the Conference on Programming for Flying Spot Devices at Bologna, October 1965, p. 219.

4) H.C. Dehne, E. Lohrmann, E. Raubold, S. Söding, M.W. Teucher, G. Wolf, Phys. Rev. 136, B 843 (1964).

5) T. Ferbel, A. Firestone, J. Sandweiss, H.D. Taft, M. Gailloud, T.W. Morris, W.J. Willis, A.H. Bachman, P. Baumel, R.M. Lea, Phys. Rev. 138, B 1528 (1965).

6) E.L. Hart, R.I. Louttit, T.W. Morris, Phys. Rev. Letters 9, 133 (1962).

7) E. Pickup, D.R. Robinson, E.O. Salant, Phys. Rev. Letters 8, 329 (1962).

8) R. Kraemer, L. Madansky, M. Meer, M. Nussbaum, A. Pevsner, C. Richardson, R. Strand, R. Zdanis, T. Fields, S. Orenstein, T. Toohig, Phys. Rev. 136, B 496 (1964).

9) T.C. Bacon, W.J. Fickinger, D.G. Hill, H.W.K. Hopkins, D.K. Robinson, E.O. Salant, preprint, presented at the topical Conference on Resonant Particles at Athens, Ohio, June 1965.

10) K. Böckmann, B. Nellen, E. Paul, I. Borecka, J. Diaz, U. Heeren, V. Liebermeister, E. Lohrmann, E. Raubold, P. Söding, S. Wolff, S. Coletti, J. Kidd, L. Mandelli, V. Pelosi, S. Ratti, L. Tallone, Phys. Letters 15, 356 (1965); and V. Alles-Borelli, B. French, Å. Frisk, L. Michejda to be published.

11) M. Ferro-Luzzi, R. George, Y. Goldschmidt-Clermont, V.P. Henri, B. Jongejans, D.W.G. Leith, G.R. Lynch, F. Muller, J.-M. Perreau, Nuovo Cimento 39, 417 (1965).

PS/5438/rmn

12) B.E.Y. Svensson, Nuovo Cimento 39, 667 (1965).

13) G. Goldhaber, J.L. Brown, I. Butterworth, S. Goldhaber, A.A. Hirata, J.A. Kadyk, B.C. Shen, G.H. Trilling, Physics Letters 18, 76 (1965).

14) L. Stodolsky, J.J. Sakurai, Phys. Rev. Letters 11, 90 (1963).

Figure Captions

Fig. 1 The $\pi^+\pi^-\pi^o$ mass distribution. The curve (thin line in the ω^o peak region) has been drawn by hand and normalized to all events except the ω^o and η^o combinations. The peak region (685-880 MeV) has been fitted with a straight line plus a Breit-Wigner curve which is shown as a thick line.

Fig. 2 Production angular distribution of ω^o mesons. The full line histogram shows the peak events while the dashed one is made for events from adjacent regions.

Fig. 3 Dalitz plot for the $\bar{p}p\omega$ final state.

Fig. 4 (a) Chew-Low plot for the $\bar{p}p\omega$ final state.

(b) Its mass projection compared with a phase space curve. Each event is plotted twice.

Fig. 5 Decay angular distributions of omega mesons. Angle θ' is the angle between the normal to the decay plane and the incident $\bar{p}$ or the target proton direction (see text) transformed to the ω rest frame. Smooth curves are of the form $1 + B\cos^2\theta'$, the fitted values of B being shown.

(a) Full line histogram shows the distribution for the 253 peak events. The dotted line is the distribution for enlarged adjacent region normalized to 89 background events.

(b) Lower distribution is for events where the smaller of the 2 masses $M_{p\omega}$, $M_{\bar{p}\omega}$ was below 1.98 GeV, upper one shows the rest of events.

PS/5438/rmn

Fig. 5 (c) Lower histogram is for events in which the lighter of the $\bar{p}\omega$, $p\omega$ systems has a momentum transfer $-t < 0.5$ $(GeV/c)^2$, upper one shows events with higher t values.

Fig. 6 Feynman graphs for the process $\bar{p}p \longrightarrow \bar{p}p\omega^o$.

Fig. 7 The $p\pi^+$ mass vs. the $\bar{p}\pi^-$ mass scatter plot for 2009 events of the channel (1) which are outside the ω^o and η^o regions.

Fig. 8 The $p\pi^+$(a) and $\bar{p}\pi^-$(b) mass distributions for 2009 events of channel (1) which are outside the ω^o and η^o regions. The smooth thick lines show the result of the fit (7). The thin lines show the phase space mass distributions for the 5-body channel (6c) added to one of the 4-body channel (6a) or (6b) distributions when projected on to the axis other than that corresponding to the resonating pair.

Fig. 9 Angular c.m. distributions for N^*(a), π^o mesons (b) and $\bar{N}^*$(c) produced in the reaction $\bar{p}p \rightarrow N^*\bar{N}^*\pi^o$.

Fig. 10 Dalitz plot for the $\bar{N}^*$ N^* π^o final state.

Fig. 11 Mass distribution of the $\bar{N}^*\pi^o$ and $N^*\pi^o$ systems in the channel (3).

Fig. 12 Decay angular distributions for the N^*, $\bar{N}^*$ isobars. Angle θ' is defined as the angle between the target p or the incident $\bar{p}$ momentum transformed to the isobar rest frame and the momentum of the nucleon resulting from the isobar decay. The full line shows the distributions for 212 clean N^* $\bar{N}^*$ π^o events, a continuous line the result of a least square fit and the dashed line the background distributions which were subtracted from the total distributions.

(a) Overall distribution for all N^*, $\bar{N}^*$ isobars.

(b) Lower histogram is for isobars which make a bigger mass with the π^o meson, upper for isobars which make a smaller mass.

Fig. 12 (c) Lower histogram is for isobars which are associated with their partner isobar decaying under large angles, upper for isobars for which accompanying isobar decays under small angle (no restriction on $N^{*}\pi^{o}$, $\bar{N}^{*}\pi^{o}$ mass).

Fig. 13 Feynman graphs for the reaction $\bar{p}p \longrightarrow N^{*}\bar{N}^{*}\pi^{o}$.

Fig. 14 Scatter diagram for the reaction $\bar{p}p \rightarrow N^{*}\bar{N}^{*}\pi^{o}$ where $\cos\theta'_1$, the decay angle for the isobar making a higher mass with the π^{o} meson ("free" isobar) is plotted versus $\cos\theta'_2$, the decay angle of its partner isobar. Projections (full line) are made after subtracting background distributions (shown with a dashed line) for 2 intervals of decay angles of the accompanying isobar.

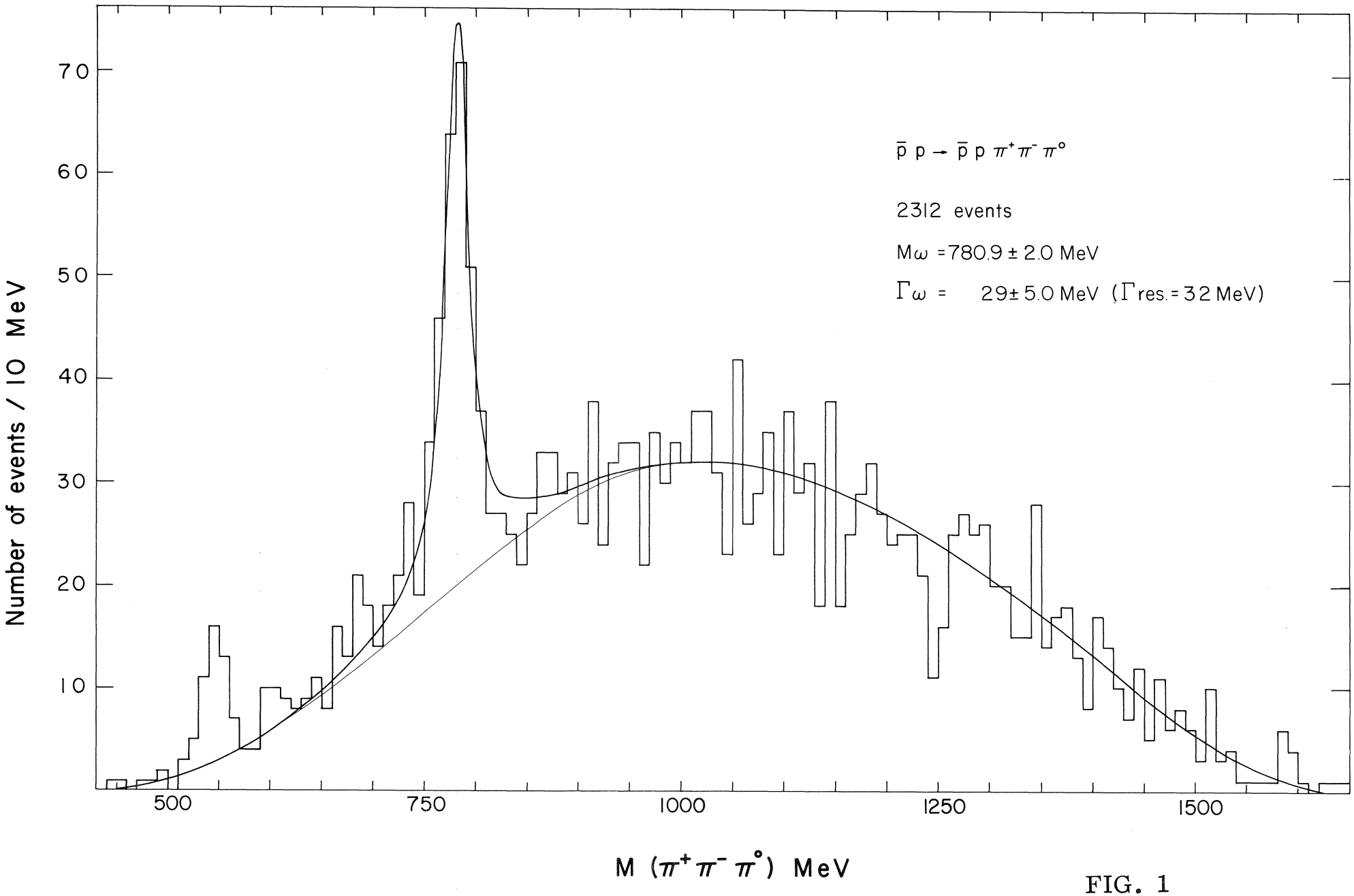

FIG. 1

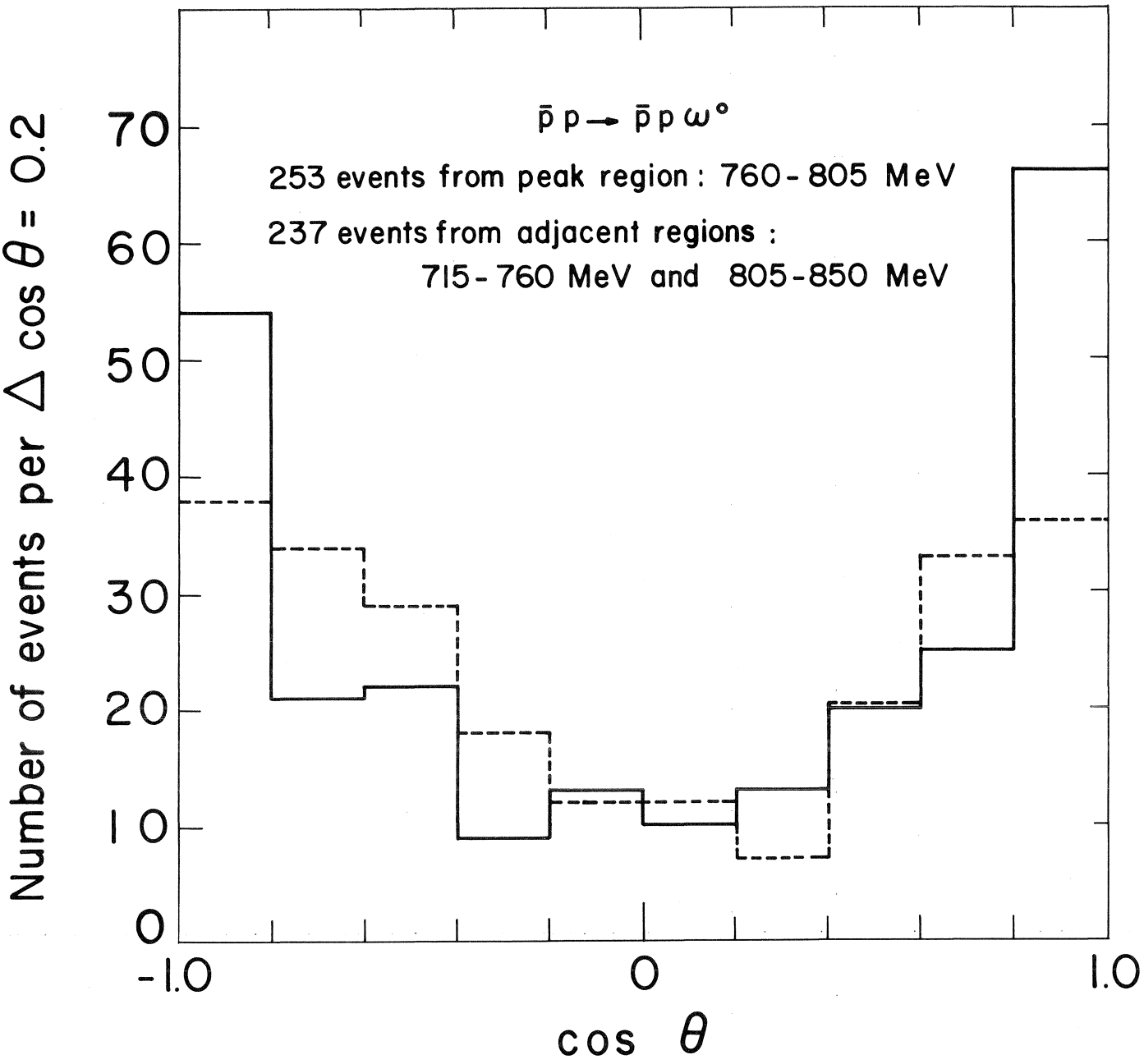
$\bar{p}\,p \rightarrow \bar{p}\,p\,\omega^{\circ}$
253 events from peak region : 760 - 805 MeV
237 events from adjacent regions :
715 - 760 MeV and 805 - 850 MeV
Number of events per $\Delta \cos\theta = 0.2$
70
60
50
40
30
20
10
0
-1.0
0
1.0
cos θ

FIG. 2

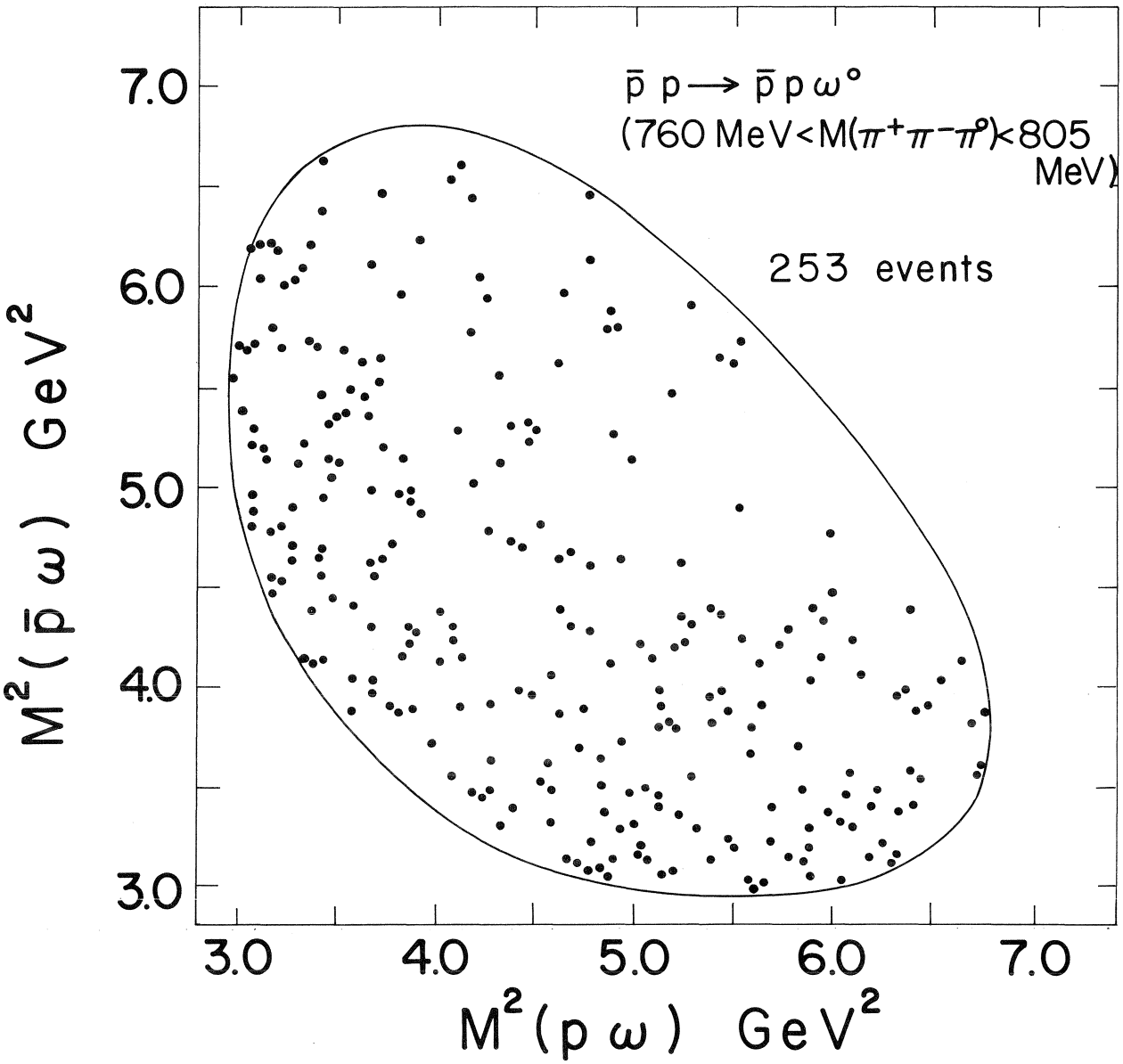
$\bar{p}\,p \longrightarrow \bar{p}\,p\,\omega^{\circ}$
(760 MeV<M($\pi^+\pi^-\pi^{\circ}$)<805 MeV)
253 events
7.0
6.0
5.0
4.0
3.0
$M^2(\bar{p}\,\omega)$ GeV^2
3.0
4.0
5.0
6.0
7.0
$M^2(p\,\omega)$ GeV^2

FIG. 3

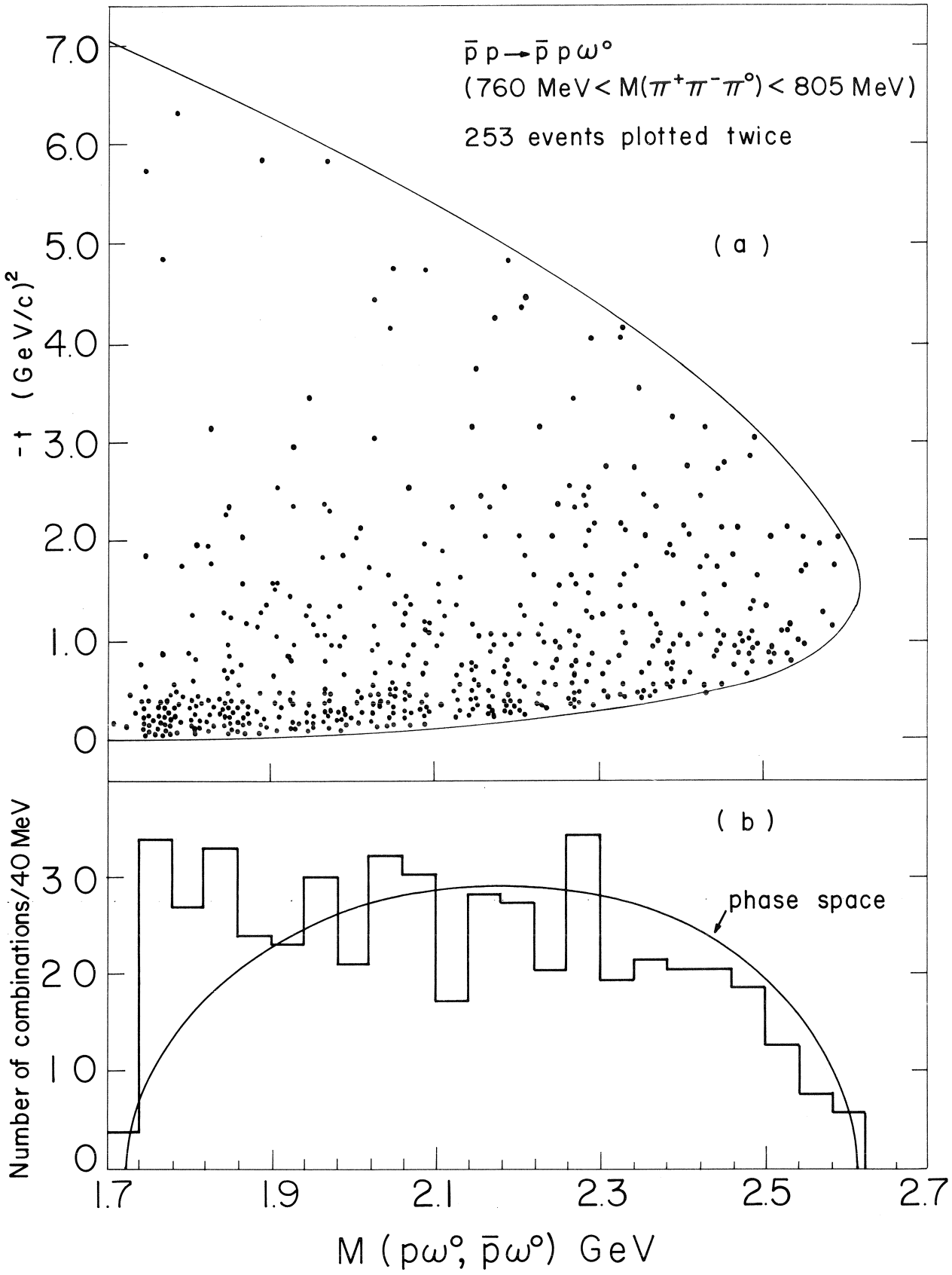
$\bar{p}\,p \rightarrow \bar{p}\,p\,\omega^\circ$
(760 MeV < M($\pi^+\pi^-\pi^\circ$) < 805 MeV)
253 events plotted twice
(a)
(b)
phase space
-t (GeV/c)^2
Number of combinations/40 MeV
M ($p\omega^\circ$, $\bar{p}\omega^\circ$) GeV
7.0
6.0
5.0
4.0
3.0
2.0
1.0
0
30
20
10
0
1.7
1.9
2.1
2.3
2.5
2.7

FIG. 4

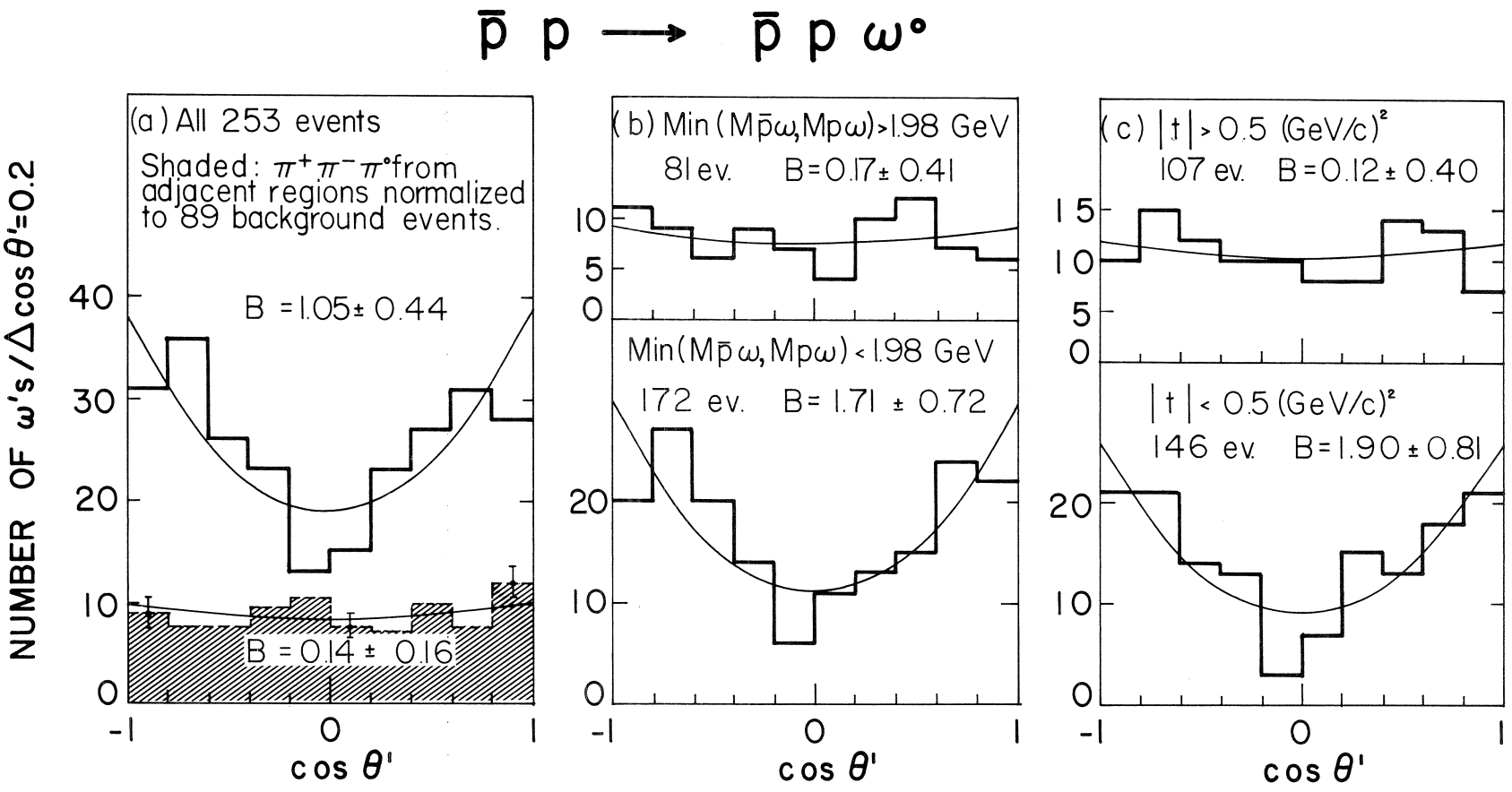
$\bar{p}\ p \longrightarrow \bar{p}\ p\ \omega^\circ$
NUMBER OF ω's/Δ cos θ'=0.2
(a) All 253 events
Shaded: $\pi^+\pi^-\pi^\circ$ from adjacent regions normalized to 89 background events.
B = 1.05 ± 0.44
B = 0.14 ± 0.16
(b) Min (Mp̄ω, Mpω) > 1.98 GeV
81 ev. B = 0.17 ± 0.41
Min (Mp̄ω, Mpω) < 1.98 GeV
172 ev. B = 1.71 ± 0.72
(c) |t| > 0.5 (GeV/c)²
107 ev. B = 0.12 ± 0.40
|t| < 0.5 (GeV/c)²
146 ev. B = 1.90 ± 0.81
cos θ'
cos θ'
cos θ'

FIG. 5

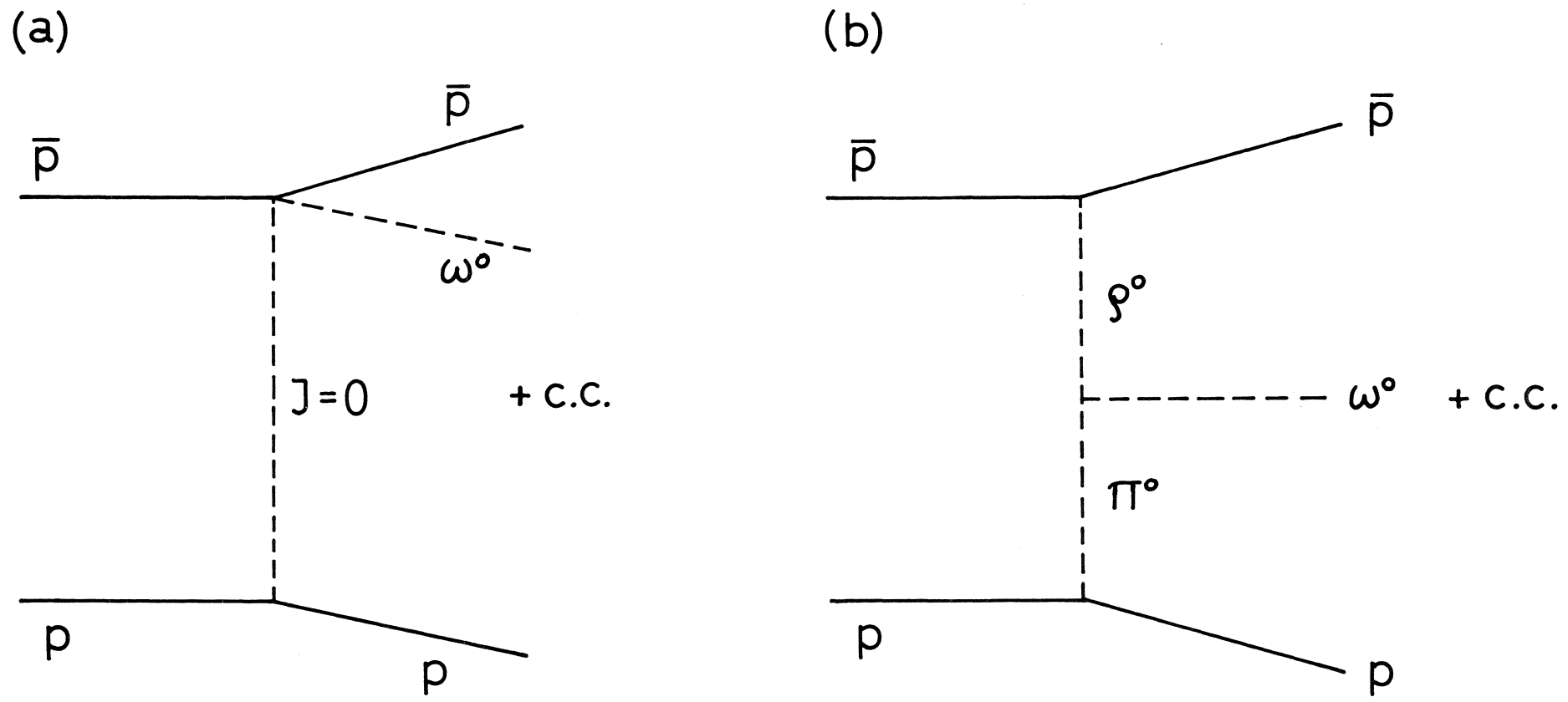
(a)
$\bar{p}$
$\bar{p}$
ω°
$J=0$
+ c.c.
p
p
(b)
$\bar{p}$
$\bar{p}$
ρ°
ω°
+ c.c.
π°
p
p

FIG. 6

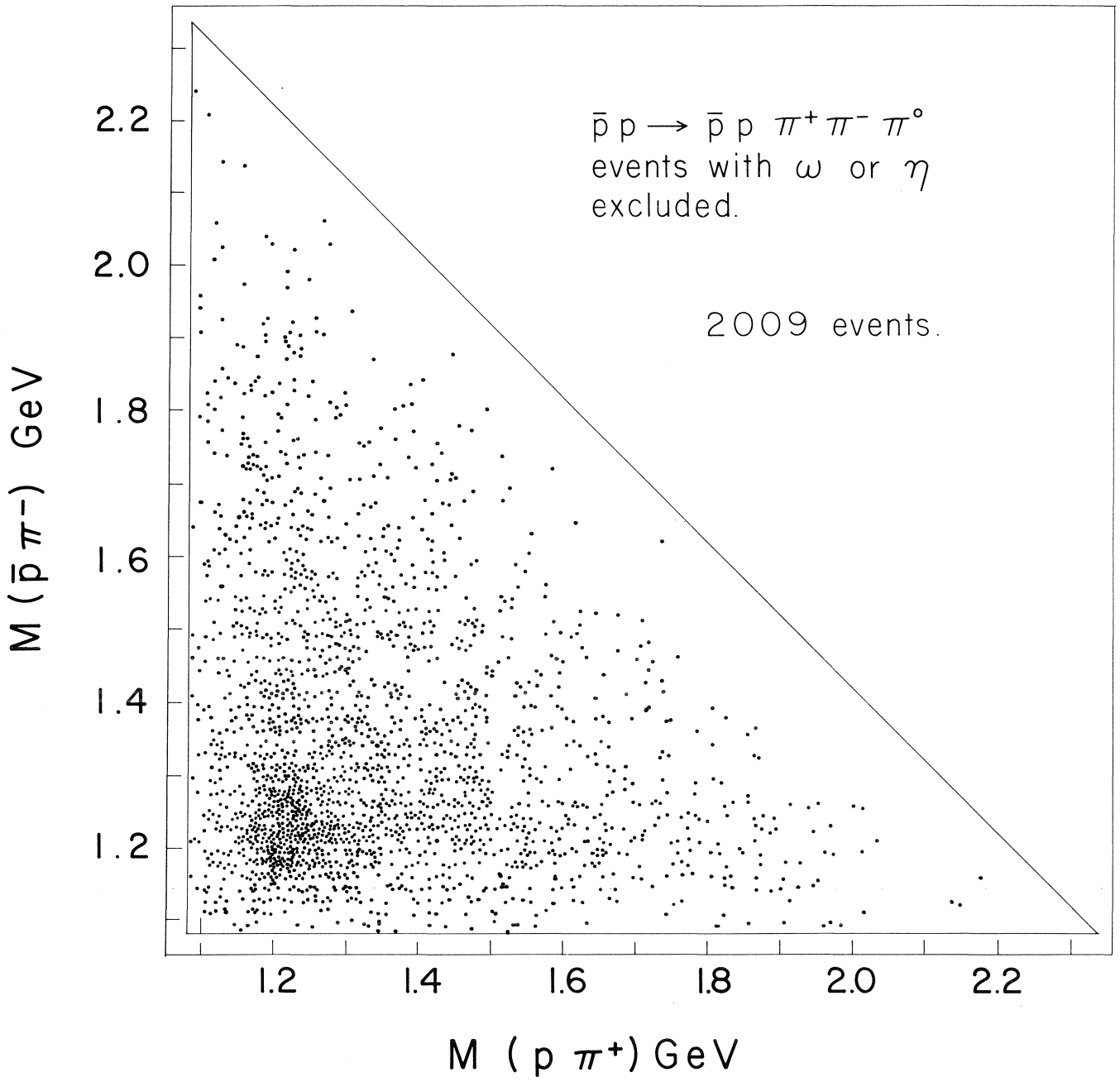
$\bar{p}\,p \longrightarrow \bar{p}\,p\ \pi^+\pi^-\pi^\circ$
events with ω or η
excluded.
2009 events.
M ($\bar{p}\,\pi^-$) GeV
2.2
2.0
1.8
1.6
1.4
1.2
1.2
1.4
1.6
1.8
2.0
2.2
M ($p\,\pi^+$) GeV

FIG. 7

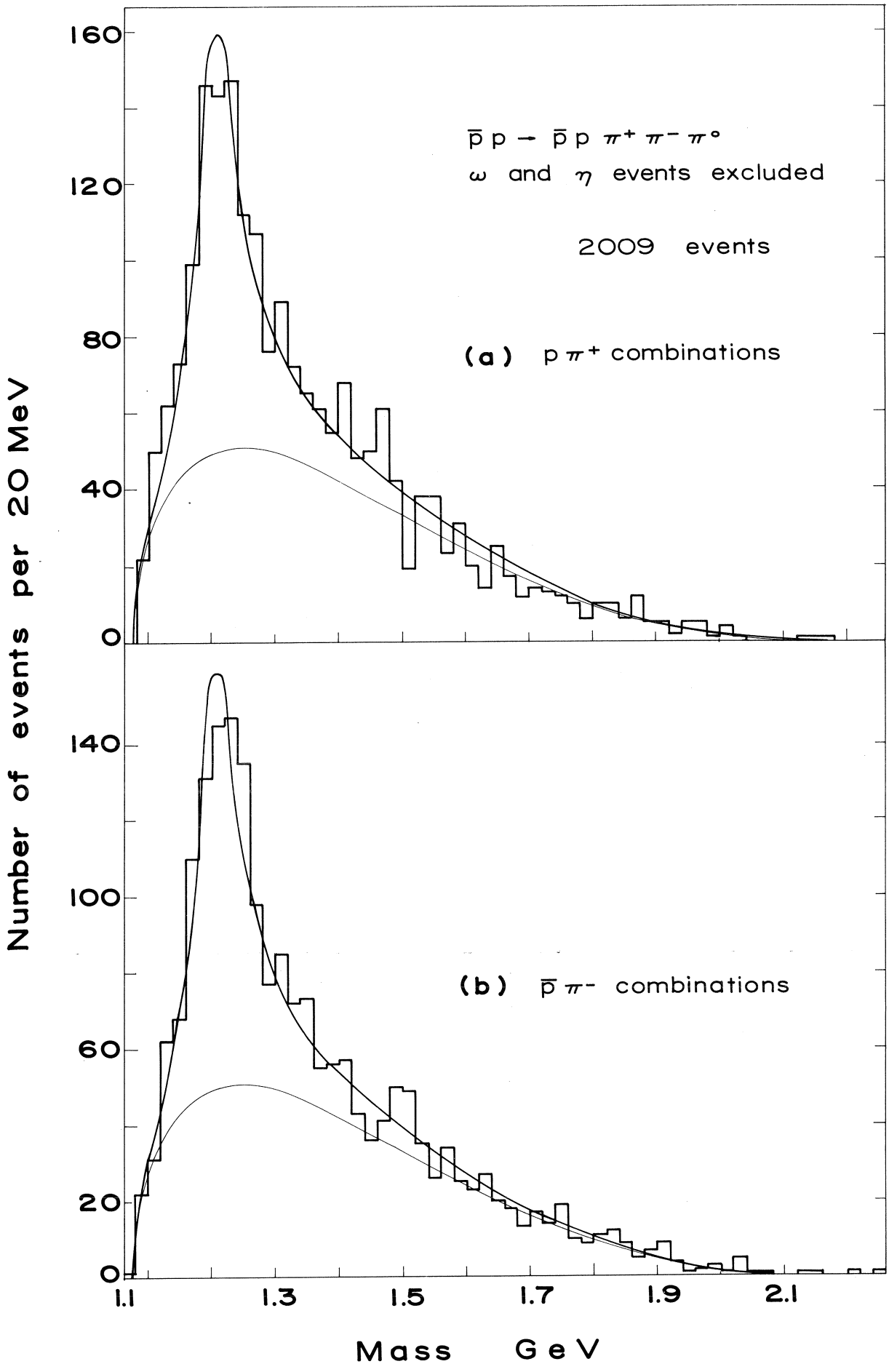
$\bar{p}\,p \rightarrow \bar{p}\,p\,\pi^+\,\pi^-\,\pi^\circ$
ω and η events excluded
2009 events
(a) $p\,\pi^+$ combinations
(b) $\bar{p}\,\pi^-$ combinations
Number of events per 20 MeV
Mass GeV
0
20
40
60
80
100
120
140
160
1.1
1.3
1.5
1.7
1.9
2.1

FIG. 8

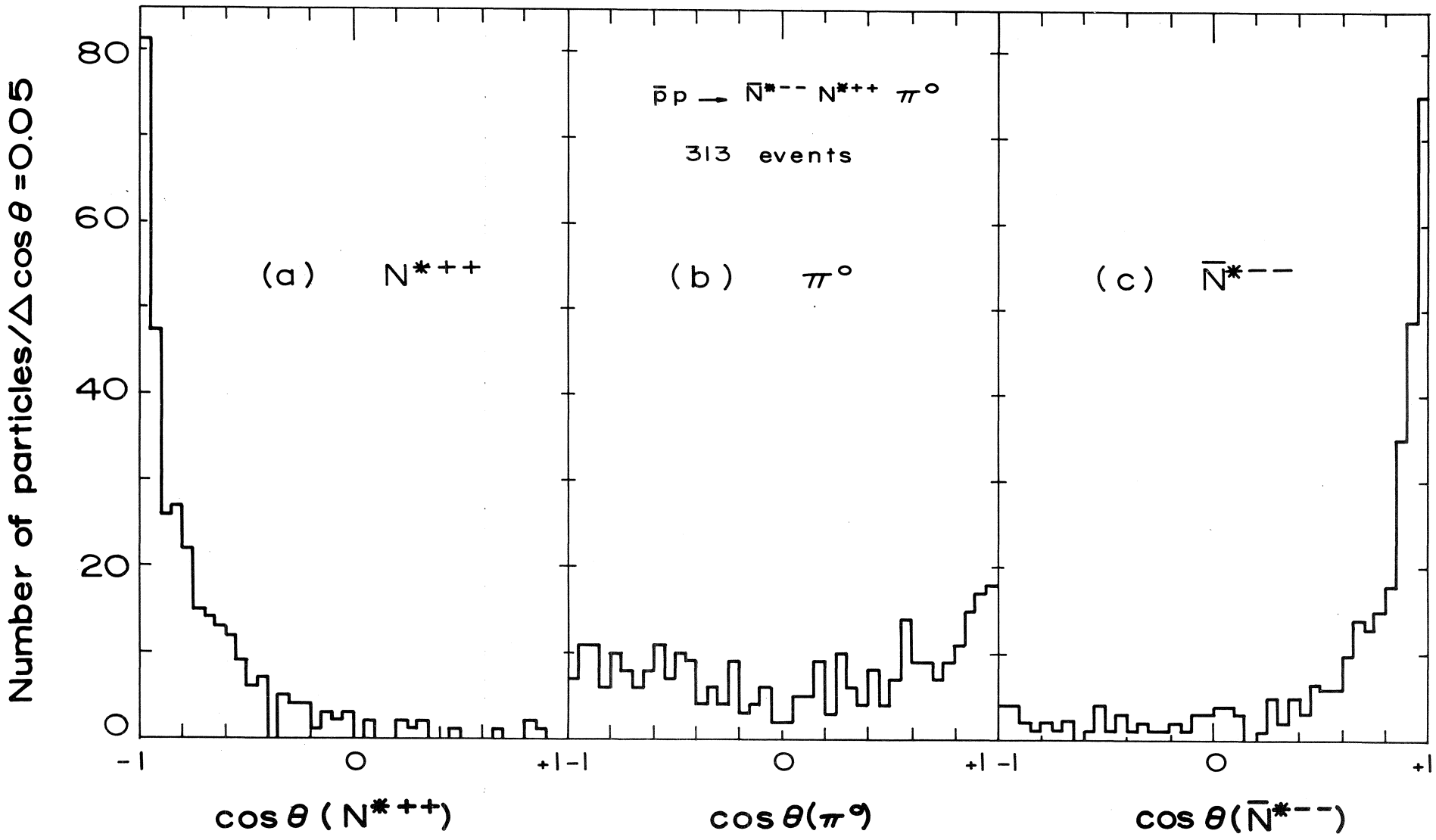
Number of particles/Δ cos θ =0.05
80
60
40
20
0
$\bar{p}p \rightarrow \bar{N}^{*--} N^{*++} \pi^0$
313 events
(a) N^{*++}
(b) π^0
(c) $\bar{N}^{*--}$
-1
0
+1
cos θ (N^{*++})
cos θ(π^0)
cos θ($\bar{N}^{*--}$)

FIG. 9

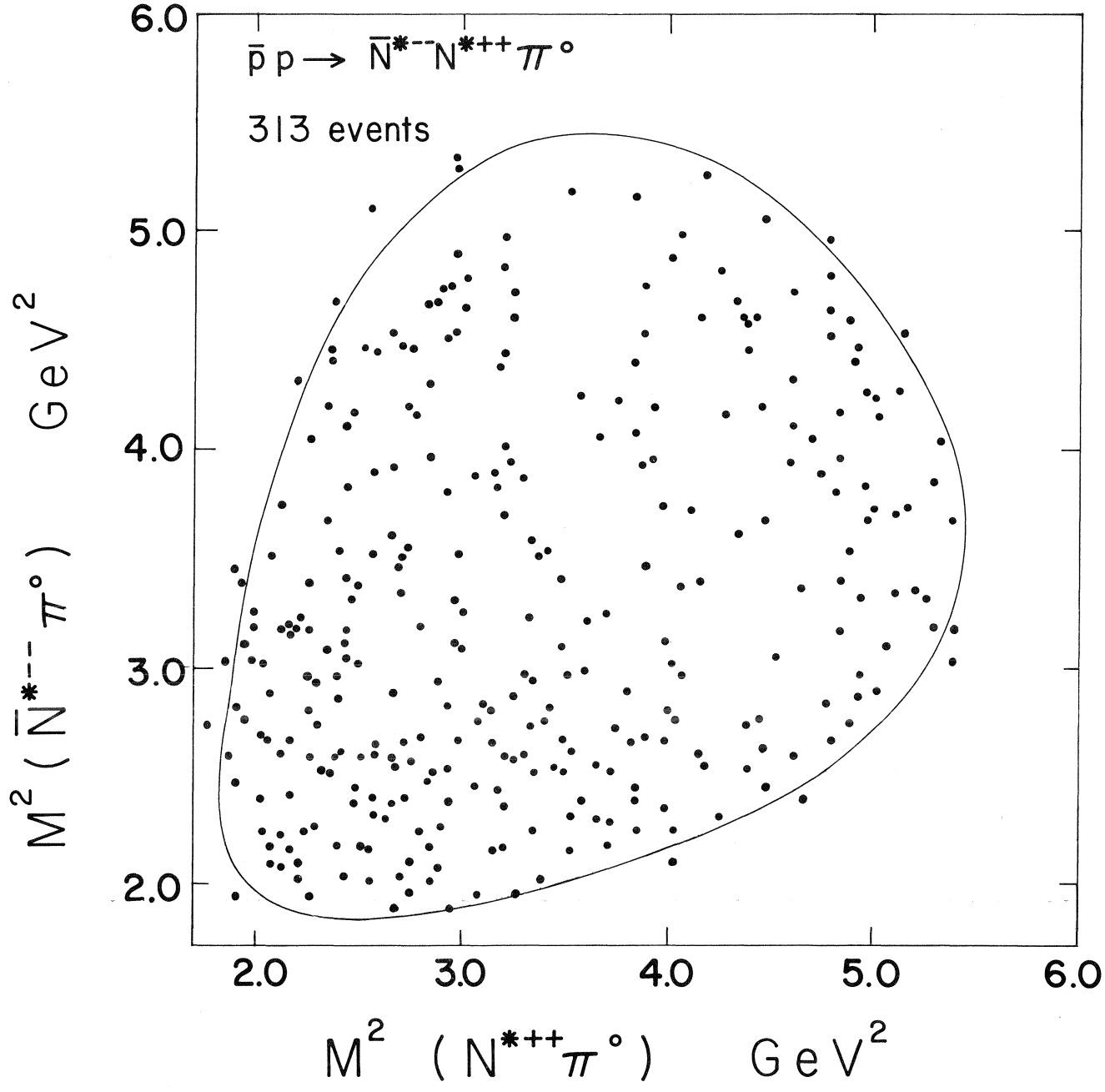
$\bar{p}\,p \rightarrow \bar{N}^{*--}N^{*++}\pi^{\circ}$
313 events
6.0
5.0
4.0
3.0
2.0
$M^2\,(\bar{N}^{*--}\pi^{\circ})$ GeV^2
2.0
3.0
4.0
5.0
6.0
$M^2\,(N^{*++}\pi^{\circ})$ GeV^2

FIG. 10

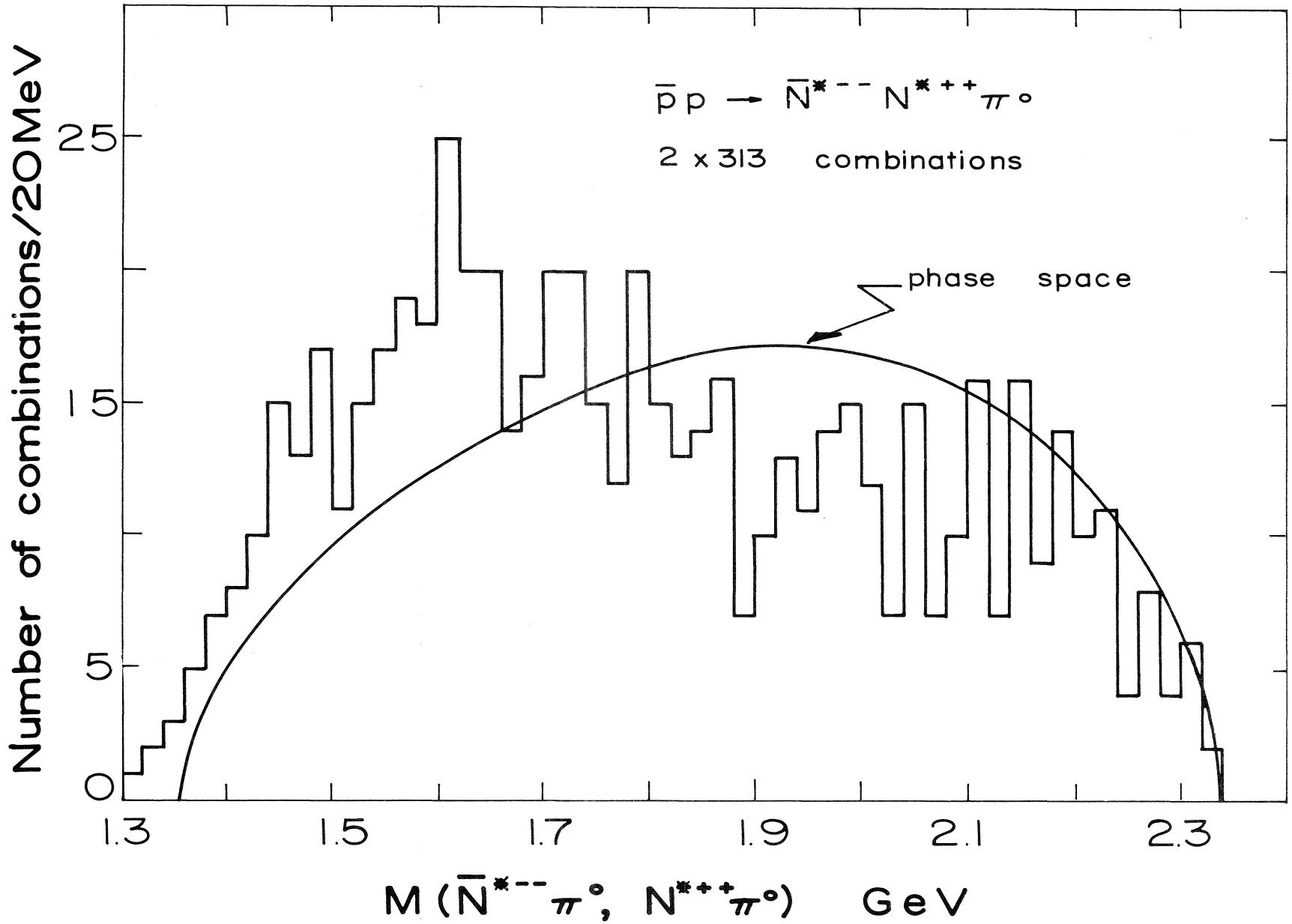
$\bar{p}p \rightarrow \bar{N}^{*--} N^{*++} \pi^{\circ}$
2 x 313 combinations
phase space
Number of combinations/20MeV
0
5
15
25
1.3
1.5
1.7
1.9
2.1
2.3
$M(\bar{N}^{*--}\pi^{\circ}, N^{*++}\pi^{\circ})$ GeV

FIG. 11

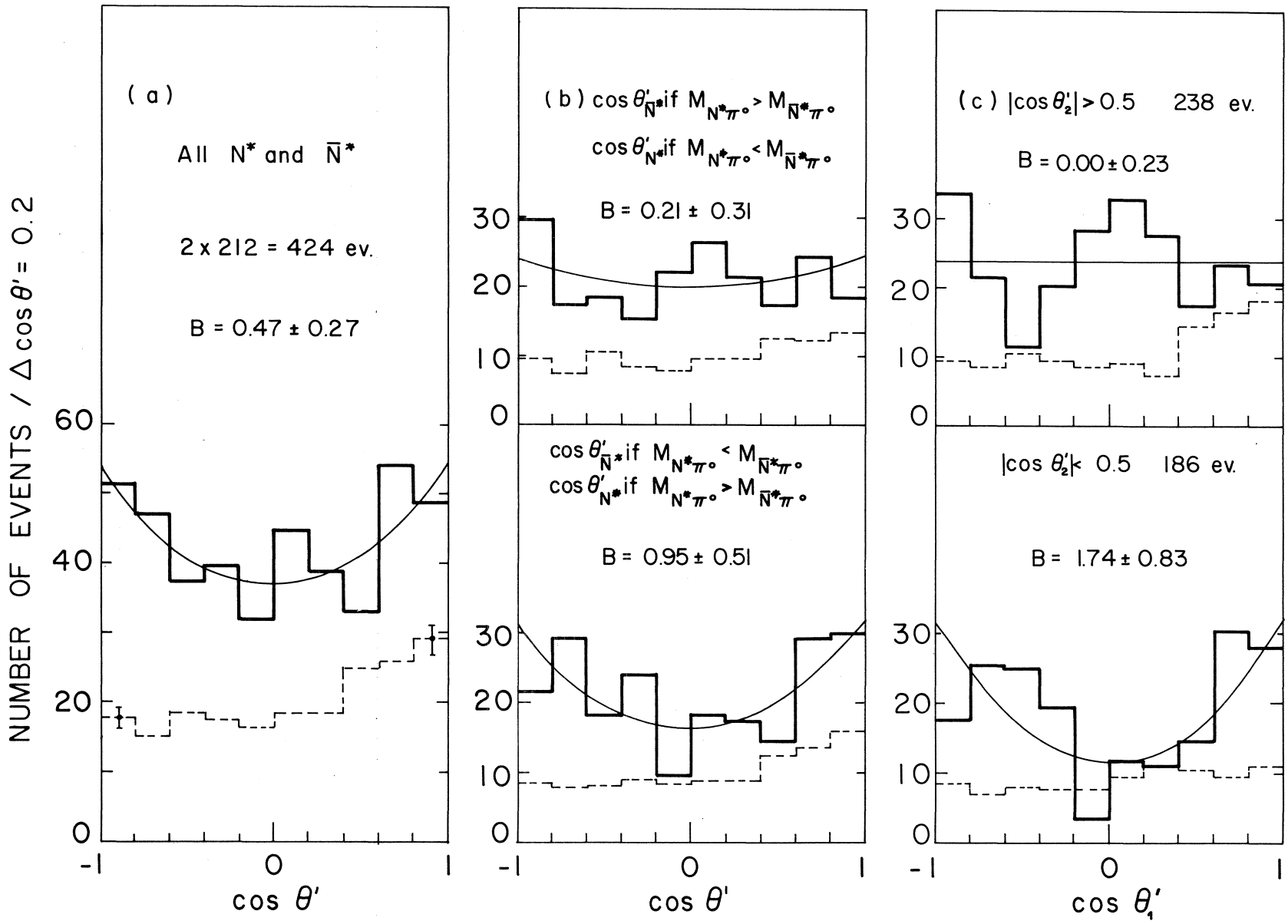
$\bar{p}p \rightarrow \bar{N}^{*--}N^{*++}\pi^{\circ}$ 212 ev. (background subtracted)
(a)
All N^* and $\bar{N}^*$
2 x 212 = 424 ev.
B = 0.47 ± 0.27
(b) $\cos\theta'_{\bar{N}^*}$ if $M_{N^*\pi^\circ} > M_{\bar{N}^*\pi^\circ}$
$\cos\theta'_{N^*}$ if $M_{N^*\pi^\circ} < M_{\bar{N}^*\pi^\circ}$
B = 0.21 ± 0.31
$\cos\theta'_{\bar{N}^*}$ if $M_{N^*\pi^\circ} < M_{\bar{N}^*\pi^\circ}$
$\cos\theta'_{N^*}$ if $M_{N^*\pi^\circ} > M_{\bar{N}^*\pi^\circ}$
B = 0.95 ± 0.51
(c) $|\cos\theta'_2| > 0.5$ 238 ev.
B = 0.00 ± 0.23
$|\cos\theta'_2| < 0.5$ 186 ev.
B = 1.74 ± 0.83
NUMBER OF EVENTS / $\Delta\cos\theta' = 0.2$
0
20
40
60
10
30
-1
0
1
cos θ'
cos θ'
cos θ'_1

FIG. 12

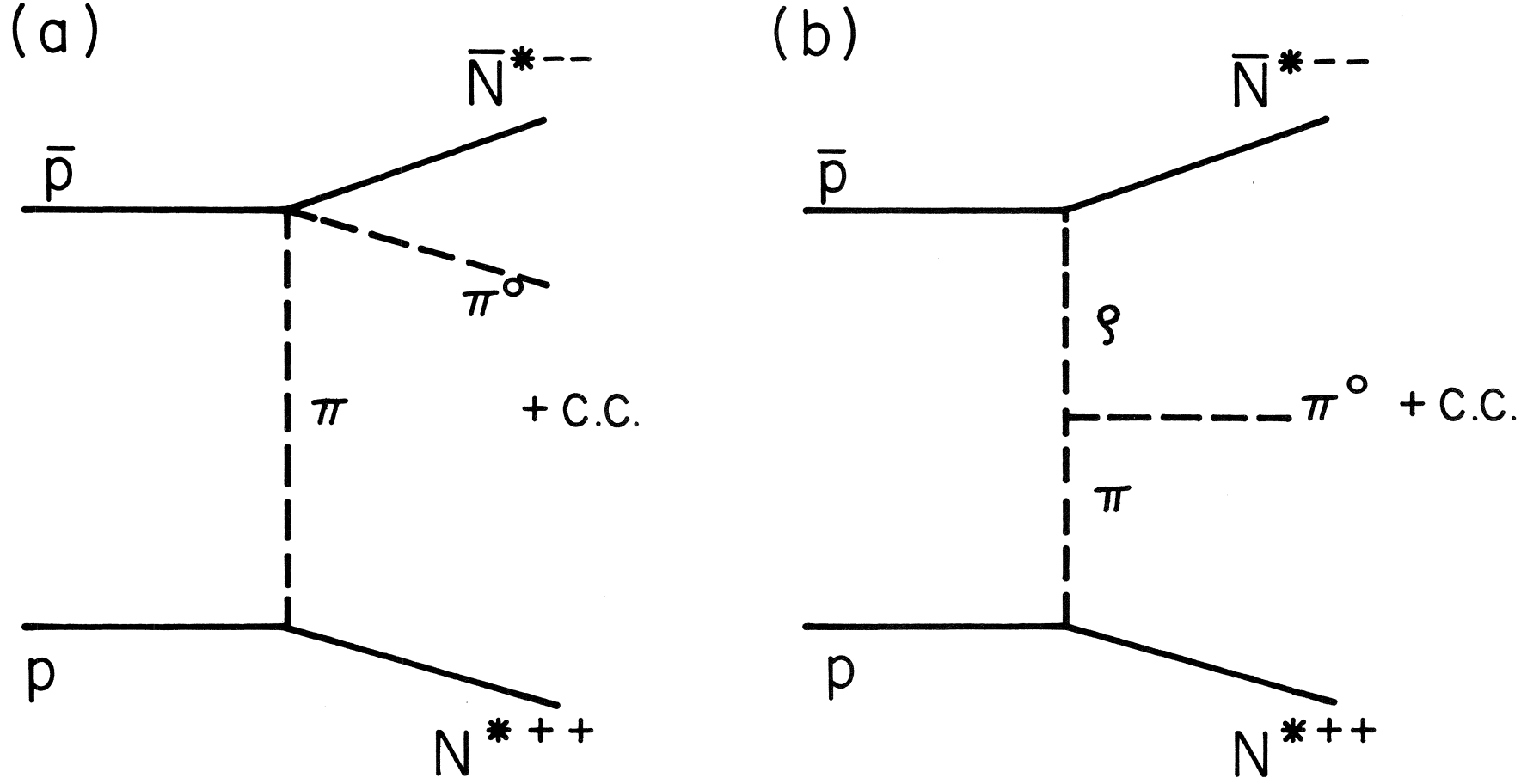

FIG. 13

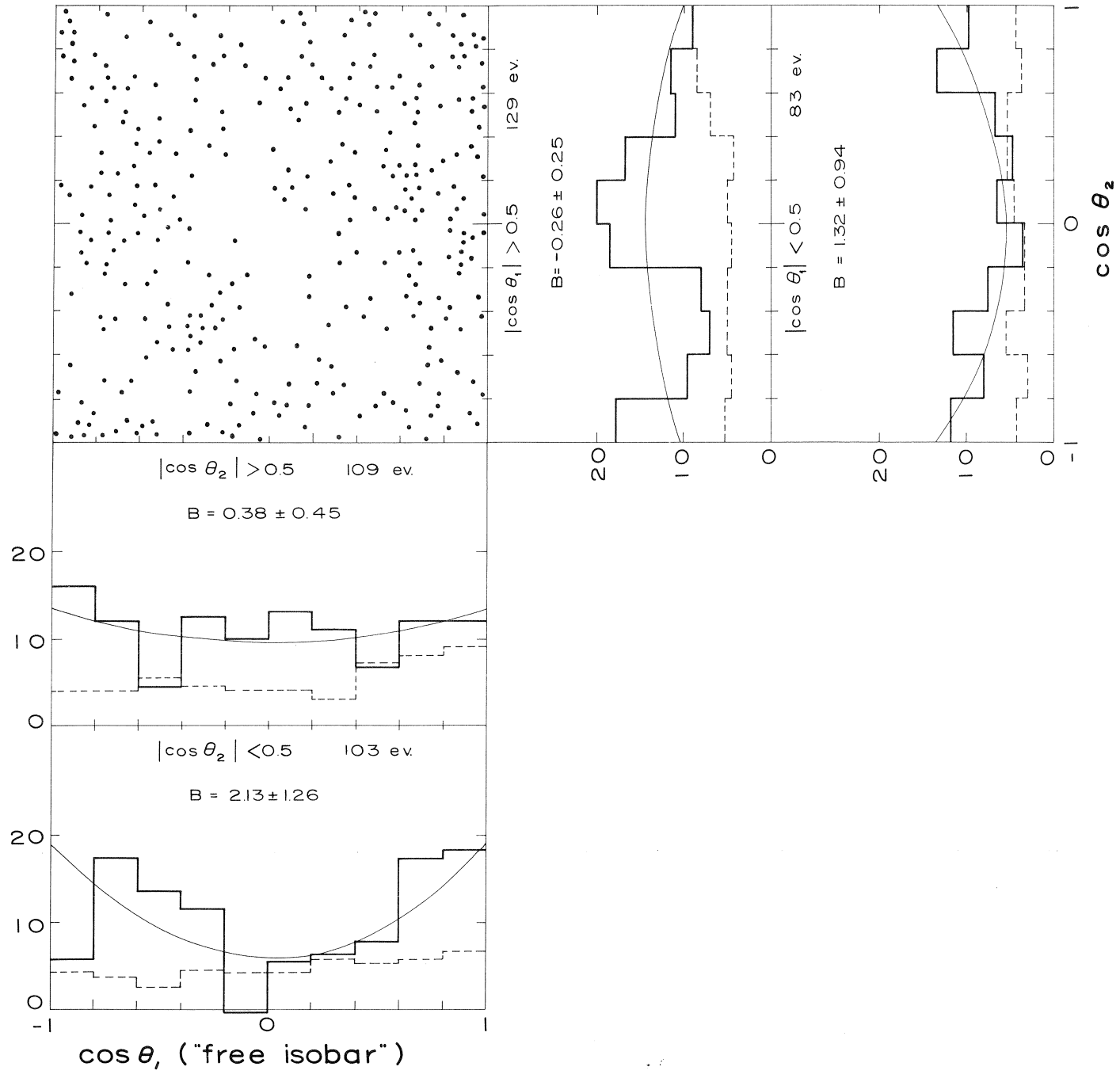
|cos θ1| > 0.5
129 ev.
B = -0.26 ± 0.25
|cos θ1| < 0.5
83 ev.
B = 1.32 ± 0.94
cos θ2
|cos θ2| > 0.5
109 ev.
B = 0.38 ± 0.45
|cos θ2| < 0.5
103 ev.
B = 2.13 ± 1.26
cos θ1 ("free isobar")

FIG. 14